Journal of Alloys and Compounds 509 (2011) 7953–7960

Contents lists available at ScienceDirect

Journal of Alloys and Compounds

journal homepage: www.elsevier.com/locate/jallcom

Effect of plane strain on microstructures and texture, through the reduction ratio of AZ31 Mg alloy

Dae-Guen Kim[a,b,*], Hyeon-Taek Son[a], Jae-Seol Lee[a], Joon-Sik Park[c]

[a] Korea Institute of Industrial Technology, 1110-9 Oryong-dong, Buk-gu, Gwangju 500-480, Republic of Korea
[b] Department of Materials Science and Engineering, Korea University, Anam-dong 5-1, Seongbuk-gu, Seoul 136-713, Republic of Korea
[c] Division of Advance Materials Engineering, Hanbat National University, Daejeon 305-719, Republic of Korea

ARTICLE INFO

Article history:
Received 2 March 2011
Received in revised form 10 May 2011
Accepted 13 May 2011
Available online 19 May 2011

Keywords:
AZ31 sheet
Plain strain
X-ray diffraction
Electron backscatter diffraction
Three-dimensional finite-element method

ABSTRACT

Structural evolution of warm-rolled AZ31 alloy sheets was investigated with respect to various reduction ratios. In order to examine the effect of rolling pass on deformation of the sheet, one-pass rolling was applied to the AZ31 alloys for various 6/1/2011reduction ratios. When the applied reduction ratio was ~85% of the initial thickness, significant grain refinement and texture development were achieved with dynamic recrystallization. Moreover, with the increase of the rolling reduction ratio from 30% to 85%, the warm rolled sheets exhibit plane strain mode displaying uniform ⟨0 0 0 1⟩//ND basal textures throughout the whole sheet thickness. The two-dimensional finite element method simulation showed that the current lubrication rolling results in a uniform plane strain deformation through the whole warm rolled sheet.

1. Introduction

The structural applications of magnesium (Mg) alloys in the automobile and aerospace industries have been steadily increasing of late due to their low density, high heat dissipation, electromagnetic shielding, and recycling. However, due to the nature of the hexagonal close-packed structure and low strength of the Mg alloys, efforts have been focused in order to identify and to increase strength and ductility via new alloy design and/or thermo-mechanical process. For the latter approach, it has been reported that the application of novel rolling process such as cross-rolling, asymmetric rolling and/or different speed rolling can effectively bias the orientation of the basal plane in the rolling plane, and can enhance the press formability, compared with conventional symmetric rolling process [1–3]. Especially, since it is well known that Mg alloys have limited number of independent active slip systems required for homogeneous deformation [4–6], the accommodating ability and ductility of Mg alloys at room temperature are generally restricted [7,8], and texture evolution in Mg alloys is largely affected by the interaction between the strain path and the initial microstructure [9,10]. Agnew and Duygulu have studied the anisotropy and hardening of AZ31 alloy under tension and showed that the deformation was initially due to the basal slip and gradually shift towards non-basal slip [11]. Jiang et al. studied the evolution of twinning under uniaxial and ring hoop tension loading at elevated temperature and concluded that the effect of twinning was more significant due to flow stress than the grain size [12]. Jain et al. have reported that the strain anisotropy (*r*-value) did not change significantly with grain size at room temperature [13]. Also, high temperature tension experiments at low strain rates were performed in order to study the superplasticity of AZ31 alloy [14–17].

While it is difficult to change the basal texture of magnesium sheet such as AZ31 and AZ61 alloys, the intensity of the basal texture can be changed, and the grain size could be reduced by controlling the rolling parameters [18,19]. For the AZ31 sheet rolled at elevate temperatures, non-basal dislocation slip and other twinning modes are easily activated in addition to basal slip and extension twinning, and the deformation mode in the AZ31 alloy sheet during hot rolling are strongly dependent on the initial grain structure and the rolling processing. In addition, continuous dynamic recovery and recrystallization (CDRR) has been reported as a phenomenon for the grain refinement and growth in Mg alloys during deformation at elevate temperatures [20,21]. Therefore, the properties of Mg alloys, such as ductility and texture development, during the rolling process will depend on the rolling method and conditions, such as the rolling temperature, rolling direction, and reduction ratio. Recently, regarding to the high deformation amount during rolling, it has been reported that

* Corresponding author at: Korea Institute of Industrial Technology, 1110-9 Oryong-dong, Buk-gu, Gwangju 500-480, Republic of Korea. Tel.: +82 62 6006291; fax: +82 62 6006149.
E-mail address: dgkim7@kitech.re.kr (D.-G. Kim).

0925-8388/$ – see front matter © 2011 Elsevier B.V. All rights reserved.
doi:10.1016/j.jallcom.2011.05.048

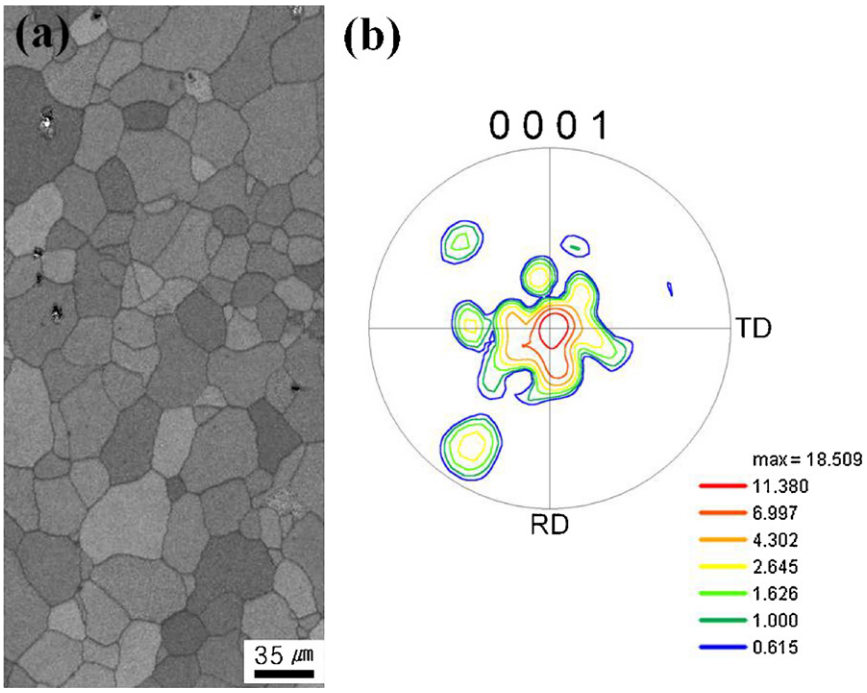

Fig. 1. (a) Optical microstructure of the as-received AZ31 Mg alloy, (b) {0 0 0 2} pole figure of the as-received sheet.

high reduction ratio has been preferred for achievement of high strength and ductility, since high stored energy leads to high driving force for nucleation, resulting in fine grain structure [22,23]. While the aforementioned analyses have given an insight for controlling deformation path and microstructures, there are still structural inhomogeneities for the rolled sheets due to the nature of the rolling process i.e., different deformation modes are applied for surface and central part of the rolled sheet [19,24]. Furthermore, when multiple rolling times were applied on the sheet for accomplishing large amount of deformation, unnecessary complexity may arise due to the different amounts of applied deformation for each rolling step.

In the present study, a central focus has been given to investigate the AZ31 rolling process that can achieve plane strain condition through the whole sample thickness using a conventional rolling mill. Also, for the first time, in order to remove any complexity during the rolling process, the deformation was applied by one single pass of rolling from 30% to 85% reduction ratio. Followed by the rolling process, the microstructures and texture evolution of the center and surface part were distinctly investigated using optical micrography (OM) and electron backscatter diffraction (EBSD) before and after heat treatments. The two-dimensional finite-element method (FEM) simulation was used for identification of strain mode estimation of the rolling process by lubrication.

2. Experimental procedures

The initial sample size of the commercial AZ31 alloy sheet was about $120 \times 100 \times 4$ (length, width and height) mm. The alloy sheet was heated to 573 K, after which it was warm-rolled using a laboratory rolling mill with a roll diameter of 300 mm and a speed of 19 m/min. The warm-rolling was carried out by one single pass. The thickness after one single pass was measured as 2.8, 2.0, 1.2 and 0.7 mm thicknesses, corresponding to 30, 50, 70 and 85% thickness reduction ratio, respectively. The rolling condition was experimented so that the plane strain can operate in the whole sample thickness depending on the lubrication condition. In order to determine the variation of the texture through the thickness, X-ray texture measurements were performed. In this study, in order to denote the position of the plate (i.e., center or surface of the plate) the location were characterized by the s parameter ranging from 0.0 to 1.0. The thickness parameter (s) was used to represent the position of the layer, where $s = 1.0$ denotes the sheet surface and $s = 0.0$ the sheet center.

The microstructure of the rolled samples was examined via optical microscopy (OM). The specimen for OM observations was polished with SiC papers and colloidal silica. The etchant was prepared with a solution of ethanol (100 ml), picric acid (5 g), acetic acid (5 ml), and water (10 ml). Finally, the samples were cleaned with methanol and were dried. The average grain sizes were measured via the linear intercept method and EBSD (electron backscatter diffraction). In order to interpret the distribution of the strain in the roll gap during plane-strain rolling, FEM simulations were performed, using the rigid-plastic FEM code DEFORM. The FEM calculation of friction parameter m was used, where m was defined as the ratio of the frictional stress to the critical stress, and $m = 1$ denotes sticking. As high friction without lubrication prevailed during rolling without lubrication, $m = 0$ was assumed between the sample surface and the rolls [9].

3. Results and discussion

Fig. 1(a) and (b) shows the microstructure and pole figure, respectively, of the RD–TD of the as-received sheet. It is noted that the microstructure was very homogeneous and had fully equiaxed grains. The average grain size was 29.4 μm, measured via EBSD and the linear intercept method, and the initial pole figure shows {0 0 0 1}//ND of the typical recrystallized Mg alloy.

Fig. 2 shows the microstructures of the plane-strain-rolled AZ31 alloy samples without annealing: (a and b) 30% rolling reduction ratio; (c and d) 50% rolling reduction ratio; (e and f) 70% rolling reduction ratio; and (g and h) 85% rolling reduction ratio [(a, c, e and g) center part; (b, d, f and h) surface part]. At 30% reduction ratio, many twins were found on both the surface and center part, within which dynamic recrystallized (DRX) grains were observed. On the other hand, at 50% reduction ratio, the surface showed a similar behavior to that at a 30% reduction ratio. The numbers of twins were greatly reduced, however, at the center part. Moreover, DRX grains were observed mostly on the center part. It is probable that the heat loss at the roll is lower on the center layer than on the surface layer with an increased reduction ratio. Generally, the recrystallization temperature of Mg alloy is known to occur above 573 K [25–27]. With an increase in the rolling reduction ratio during warm-rolling, the significant grain refinement is observed in the AZ31 alloy. It was specially noted that a large strain rolling (70 and 85%) by one single pass decreased the grain size from 30 μm into ~2 μm, indicating that a large amount of deformation energy

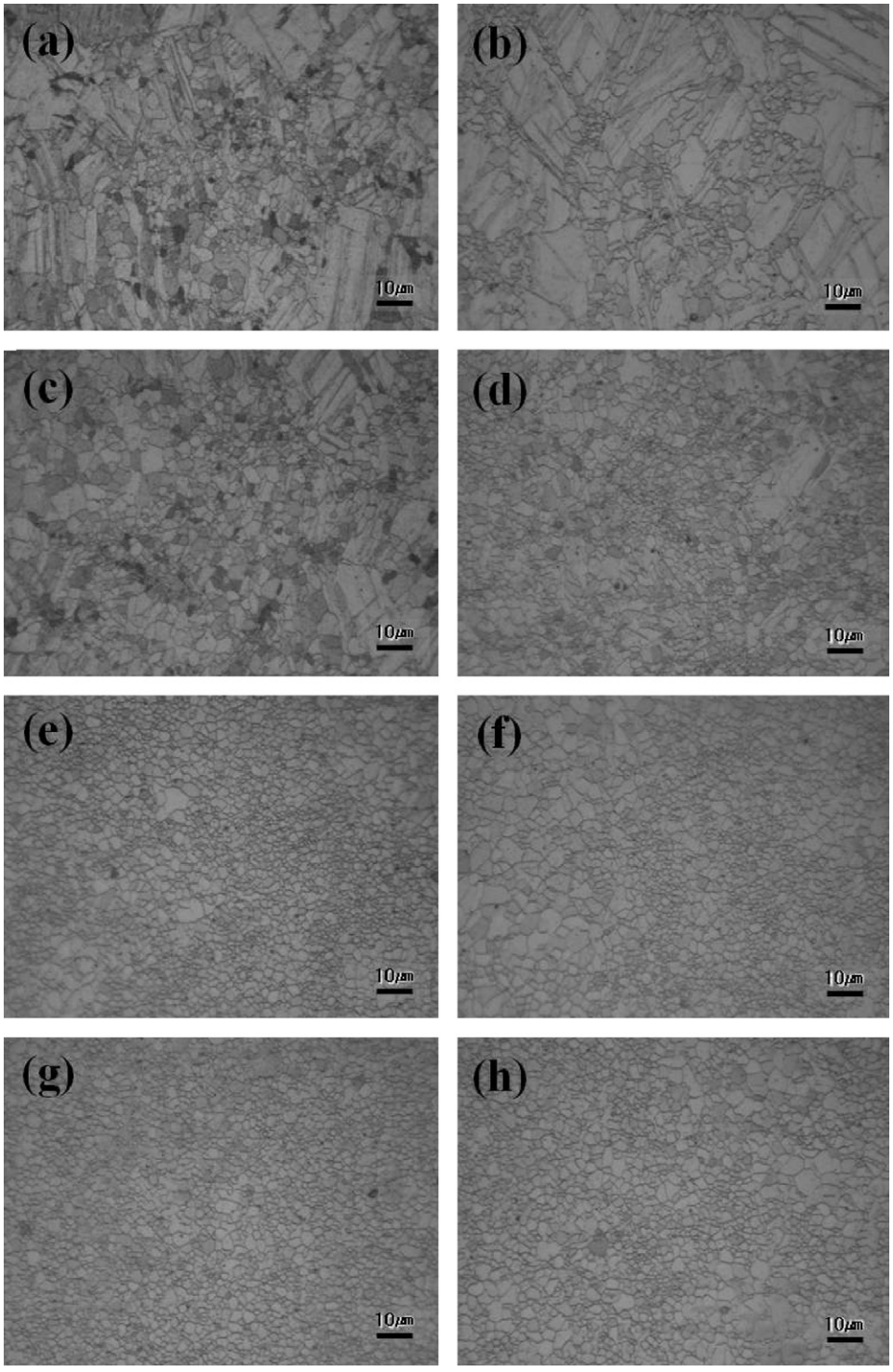

Fig. 2. The microstructures of the plane-strain-rolled AZ31 alloy samples without annealing: (a and b) 30% rolling reduction ratio; (c and d) 50% rolling reduction ratio; (e and f) 70% rolling reduction ratio; and (g and h) 85% rolling reduction ratio [(a, c, e and g) are the center part; (b, d, f and h) are the surface part].

is needed for dynamic recrystallization (DRX), when the reduction ratio is increased. The occurrence of twins is generally suppressed if the grain size is below 3 μm, since fine grains cannot concentrate large stresses and thus cannot prevent the growth of twins [28]. In the present observations, when the amount of deformation is increased, twins are hardly observed, as reported by Christian and Mahajan [28].

Fig. 3 shows the microstructure of the plane-strain-rolled AZ31 alloy samples after annealing at 573 K for 30 min: (a and b) 30% rolling reduction ratio; (c and d) 50% rolling reduction ratio; (e and f) 70% rolling reduction ratio; and (g and h) 85% rolling reduction ratio [(a, c, e and g) center part; (b, d, f and h) surface part]. For the specimens with 30 and 50% reduction ratios, the produced twins were fully recrystallized after annealing. However, for the specimens with 70 and 85% reduction ratios, grain growth was observed after annealing, indicating that the recrystallization was completed right after warm rolling.

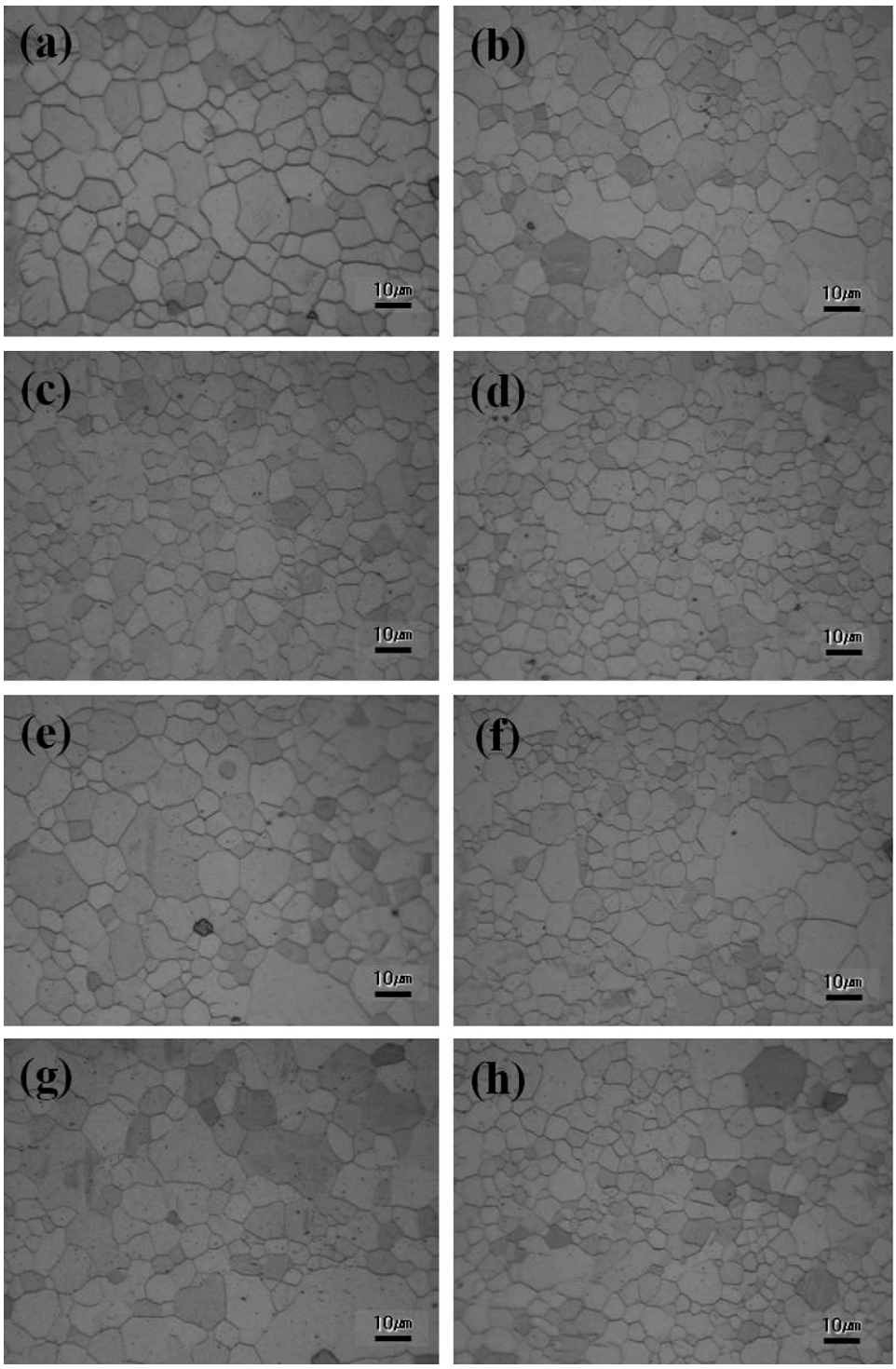

Fig. 3. Microstructures of the plane-strain-rolled AZ31 alloy samples after annealing at 573 K for 30 min: (a and b) 30% rolling reduction ratio; (c and d) 50% rolling reduction ratio; (e and f) 70% rolling reduction ratio; and (g and h) 85% rolling reduction ratio [(a, c, e and g) are the center part; (b, d, f and h) are the surface part].

Fig. 4 shows the (0 0 0 2) pole figures of the plane-strain-rolled AZ31 alloy samples before annealing: (a and b) initial sheet; (c and d) 30% rolling reduction ratio; (e and f) 50% rolling reduction ratio; (g and h) 70% rolling reduction ratio; and (i and j) 85% rolling reduction ratio [(a, c, e, g and i) center part; (b, d, f, h and j) surface part). The pole figures in Fig. 8(a)–(c) at ⟨0 0 0 1⟩//ND show a 7° tilt towards the rolling direction, indicating that this was caused by the formation of twins and corresponding to the microstructures shown in Fig. 2. The other figures show a typical texture of ⟨0 0 0 1⟩//ND with plane strain. It is noted that the intensity of ⟨0 0 0 1⟩//ND was reduced with an increased reduction ratio of plane strain, corresponding to the recent results reported by Jeong and Ha [29]. While our current observations agree with Mg alloys from shear strain due to the friction between the roll and the sample (i.e., conventional rolling), it should be specially noted that the DRX grains with high reduction ratio was achieved by one single pass and the AZ31 sheet was maintained plane strain condition. In addition, it is observed that the uniform ⟨0 0 0 1⟩//ND texture was obtained on both the

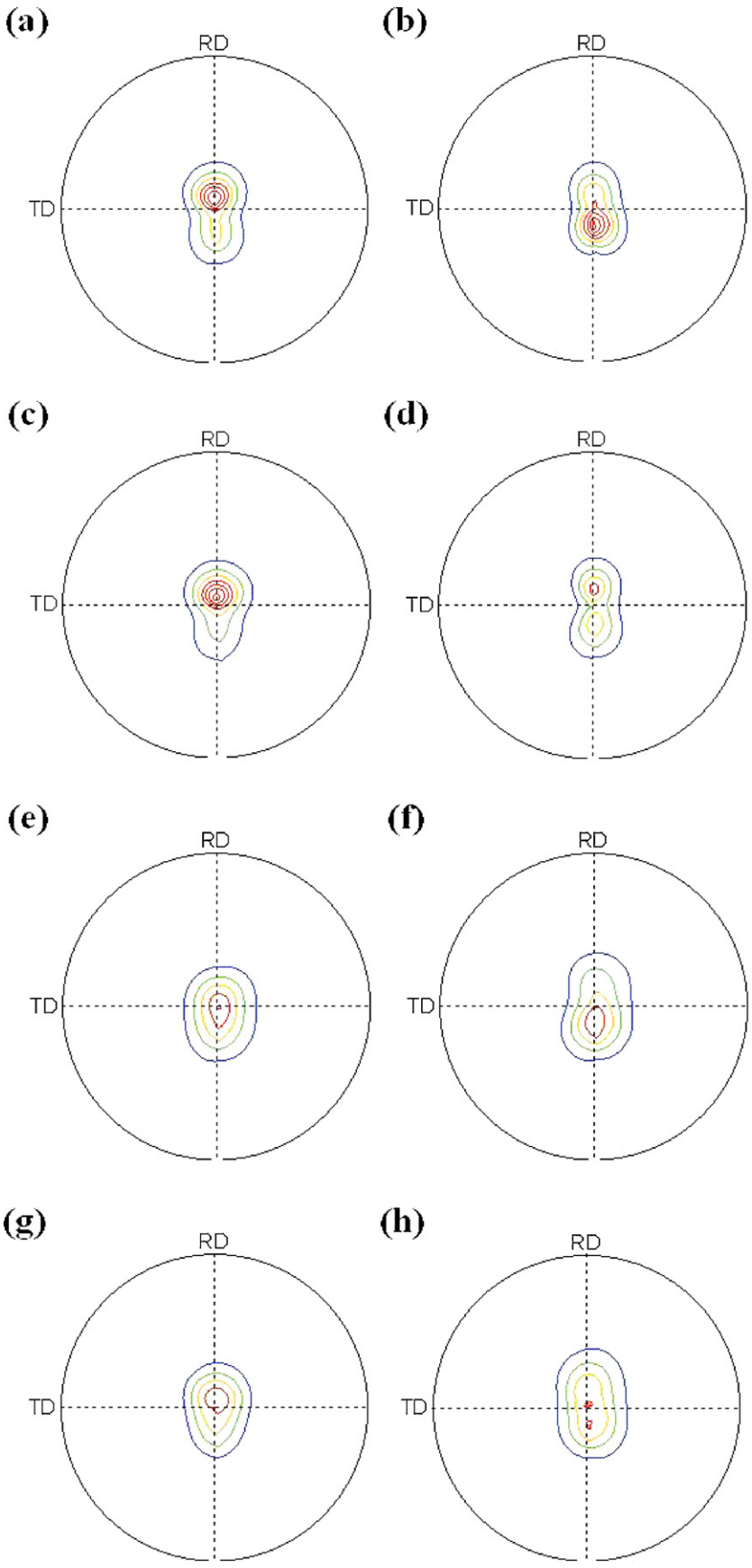

Fig. 4. (0 0 0 2) pole figures of the plane-strain-rolled AZ31 alloy samples without annealing: (a and b) initial sheet; (c and d) 30% rolling reduction ratio; (e and f) 50% rolling reduction ratio; (g and h) 70% rolling reduction ratio; and (i and j) 85% rolling reduction ratio [(a, c, e, g and i) are the center part; (b, d, f, h and j) are the surface part].

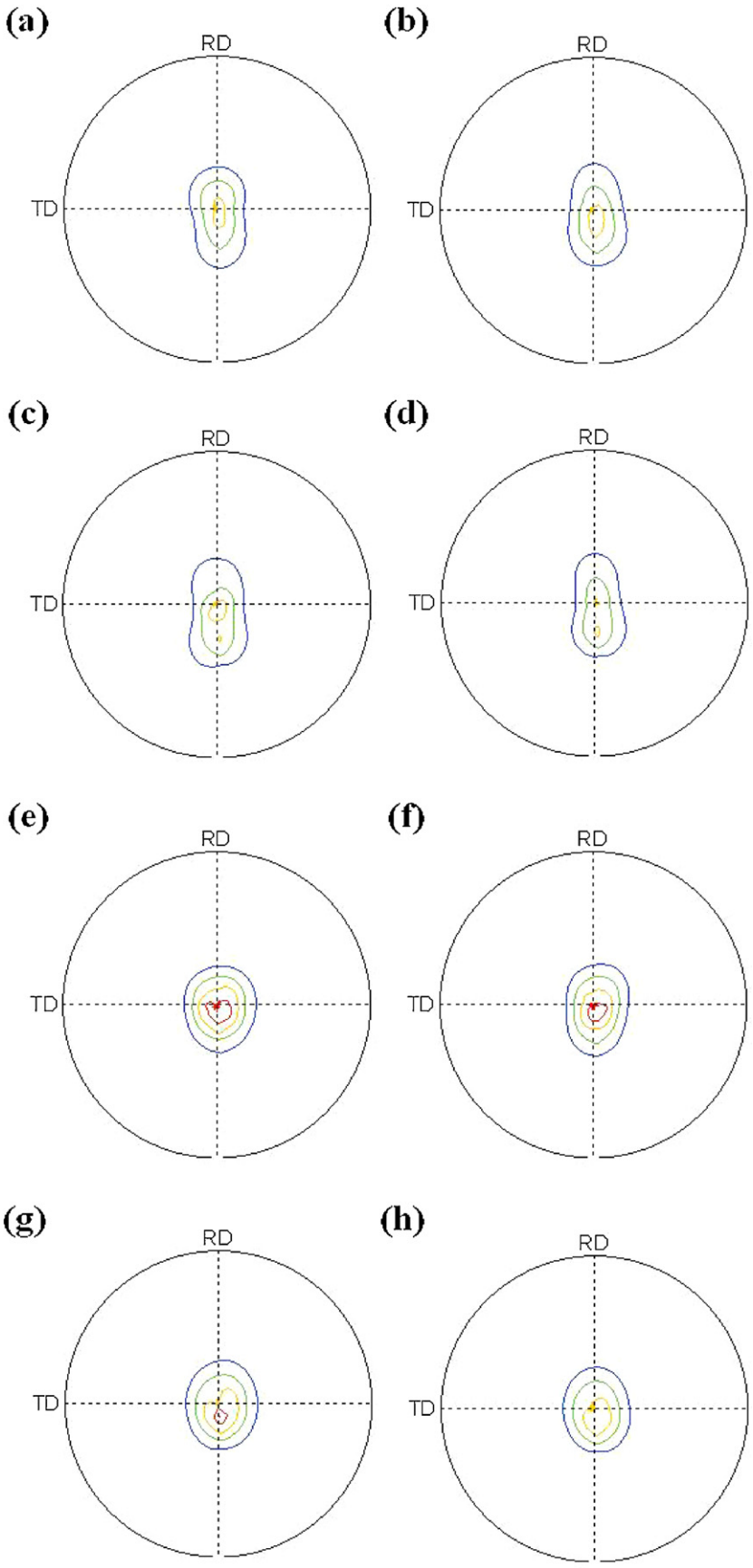

Fig. 5. (0 0 0 2) pole figures of the plane-strain-rolled AZ31 alloy samples after annealing at 573 K for 30 min: (a and b) initial sheet; (c and d) 30% rolling reduction ratio; (e and f) 50% rolling reduction ratio; (g and h) 70% rolling reduction ratio; and (i and j) 85% rolling reduction ratio [(a, c, e, g and i) are the center layers; (b, d, f, h and j) are the surface layers].

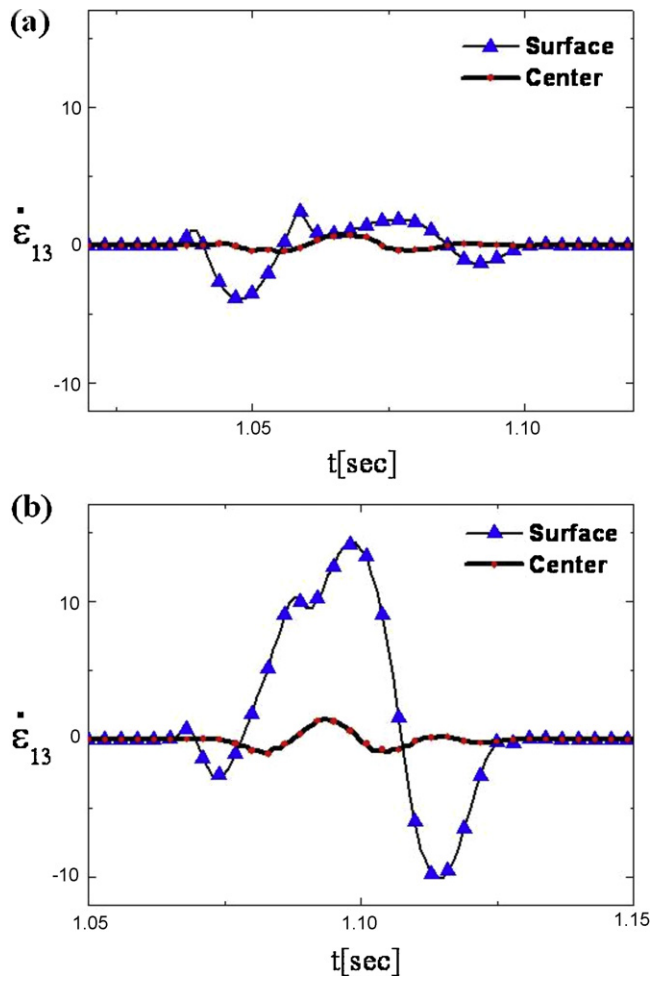

Fig. 6. Variations of shear strain rate $\dot{\varepsilon}_{13}$ within the roll gap during warm-rolling in the (a) shear strain sample and (b) plane strain sample.

center and surface part through the whole thickness of the plate, indicating that uniform deformation was applied for the designated reduction ratio during planar deformation. No difference in the texture of ⟨0 0 0 1⟩//ND was shown between the reduction ratios of 70 and 85%, implying that DRX has been completed right after rolling.

Fig. 5 shows the (0 0 0 2) pole figures of the plane-strain-rolled AZ31 alloy samples after annealing at 573 K for 30 min: (a and b) initial sheet; (c and d) 30% rolling reduction ratio; (e and f) 50% rolling reduction ratio; (g and h) 70% rolling reduction ratio; and (i and j) 85% rolling reduction ratio [(a, c, e, g and i) center part; (b, d, f, h and j) surface part). The ⟨0 0 0 1⟩//ND textures at the reduction ratios of 30 and 50% showed that the intensity of ⟨0 0 0 1⟩//ND weakened after annealing. This resulted from the recrystallization during the annealing of the twins, which were formed during rolling. At the reduction ratios of 70 and 85%, however, the textures at ⟨0 0 0 1⟩//ND had similar intensities before and after annealing. It is clear that the DRX was completed right after rolling as shown in Fig. 3. According to Perez Pardo, if considerable grain growth occurs during annealing due to the high temperature, the texture of ⟨0 0 0 1⟩//ND becomes stronger [30,31]. In this study, a similar result was obtained with the texture of ⟨0 0 0 1⟩//ND with slight grain growth during annealing at 573 K.

In the present study, the evolution of strain modes during warm-rolling was calculated from the entry to the exit of a rolling machine, via 2D FEM, using the commercial FEM package DEFORM^{TM}-3D. For details on the FEM simulation scheme regarding rolling deformation, see Refs. [32,33]. Fig. 6 shows the variations of the strain

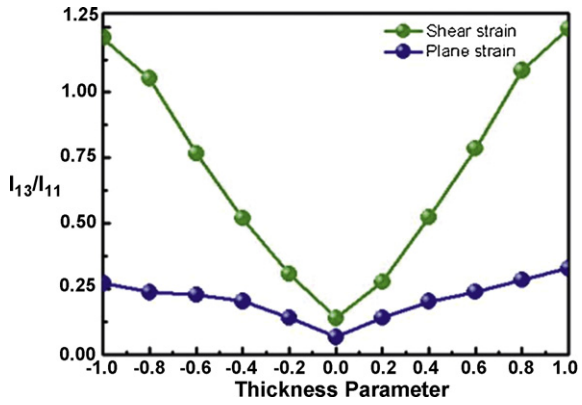

Fig. 7. Variations of I_{13}/I_{11} along the streamline for various through-thickness layers (s) in the plane strain sample.

state during the warm-rolling on the first rolling pass, by plotting shear strain rate $\dot{\varepsilon}_{13}$ along two streamlines in the sheet center (at $s = 0.0$) and close to the sheet surface (at $s = 0.8$), as a function of the FEM time. An abrupt material tilt was observed close to the surface when entering the roll gap caused the first negative peak in the variation of $\dot{\varepsilon}_{13}$ at $s = 0.8$, which occurred in both the shear and plane strain samples. Disregarding the first, shear strain rate $\dot{\varepsilon}_{13}$ in the shear strain sample was fairly low during the rolling deformation and hardly varied through the sheet thickness (Fig. 6a). In the plane strain sample, in contrast, shear strain rate $\dot{\varepsilon}_{13}$ strongly varied

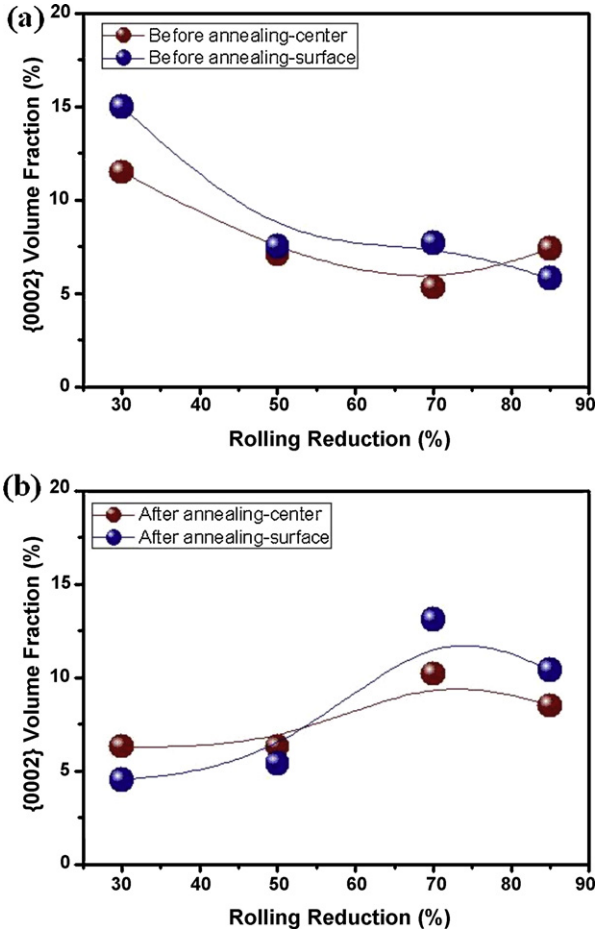

Fig. 8. Volume fraction of the crystal orientation for ⟨0 0 0 1⟩//ND on the center and surface layers by rolling reduction ratio: (a) before annealing; and (b) after annealing at 573 K for 30 min.

with the thickness parameter s; i.e., the variation in $\dot{\varepsilon}_{13}$ remarkably increased with increasing parameter s, when approaching the sheet surface (Fig. 6b). Compared with the result that was examined in the paper related to the lubrication condition in steel [34], the difference in the change on the $s = 0.8$ layer was relatively low, indicating that the plane strain can be operated in the whole-thickness layers during rolling based on the lubrication condition.

Fig. 7 shows the variation of I_{13}/I_{11} with thickness layer s for the shear and plane strain samples. In [35], it was explained that plane strain rolling texture is formed during rolling at a ratio of I_{13}/I_{11}, smaller than 0.5. Certainly, the whole-thickness layers of the present plane strain samples were operated based on a strain history, with $I_{13}/I_{11} < 0.3$.

Fig. 8 shows the volume fraction of the crystal orientation for ⟨0 0 0 1⟩//ND on the center and surface layers by rolling reduction ratio: (a) before annealing; and (b) after annealing at 573 K for 30 min. With the increase in reduction ratio before annealing, the center and surface part decreased, showing the volume fraction of the crystal orientation for ⟨0 0 0 1⟩//ND. The decrease in the volume fraction of the crystal orientation for ⟨0 0 0 1⟩//ND was due to the grain refinement and to the DRX grains produced by the high plastic energy. On the other hand, the volume fraction of the crystal orientation for ⟨0 0 0 1⟩//ND after annealing was observed to have increased from 70 and 85%, while there was decreased up to the reduction ratio of 50%. Thus, the twins remained up to the reduction ratio of 50% due to the recrystallization and grain growth during annealing. On the other hand, at the 70 and 85% reduction ratios, the grain size grew because of the grains that became fully DRX, corresponding to the microstructures and pole figure intensity of ⟨0 0 0 1⟩//ND in Figs. 3 and 4. While further investigation on structural variation at various annealing temperatures is needed, the current observations is meaningful in terms of achievement of high amount of deformation (>50%) via single path rolling and maintenance of plain strain condition during rolling.

4. Conclusions

In summary, the microstructures and texture evolution during warm-rolling with plane strain in the AZ31 alloy was investigated via optical microscopy and X-ray diffraction. The following conclusions can be drawn from this study:

(1) As the rolling reduction increased, the grain size of the rolled samples with plane strain was decreased before annealing, and the grain size decreased to around 2 μm when the rolling reduction ratios were 70 and 85%.
(2) The texture of ⟨0 0 0 1⟩//ND exhibited the same intensity on the center and surface part with plane strain. When the rolling reduction ratio increased, the texture of ⟨0 0 0 1⟩//ND developed weakly and became much weaker with fully dynamic recrystallization when the rolling reduction ratios were 70 and 85%.
(3) In the verification of the role of strain rate $\dot{\varepsilon}_{13}$ in the plane strain samples using the commercial FEM package DEFORM^{TM}-2D, the results of the FEM simulation corresponded to the experimental data.

References

[1] H. Somekawa, H. Hosokawa, H. Watanabe, K. Higashi, Mater. Sci. Eng. A 339 (2003) 328–333.
[2] W. Puschl, Prog. Mater. Sci. 47 (2002) 415–461.
[3] M.Y. Huh, S.Y. Cho, O. Engler, Mater. Sci. Eng. A 315 (2001) 35.
[4] S. Lee, Y.H. Chen, J.Y. Wang, J. Mater. Process. Technol. 124 (2002) 19.
[5] H. Takuda, T. Enami, K. Kubota, J. Mater. Process. Technol. 101 (2000) 281.
[6] H. Takuda, H. Fujimoto, N. Hatta, J. Mater. Process. Technol. 80–81 (1998) 513.
[7] M.T. Pérez-Prado, J.A. del Valle, J.M. Contreras, O.A. Ruano, Scripta Mater. 50 (2004) 661.
[8] M.T. Pérez-Prado, J.A. del Valle, O.A. Ruano, Mater. Lett. 59 (2005) 3299–3303.
[9] L. Jin, W.Y. Wu, R.K. Mishra, A.A. Luo, A.K. Sachdev, S.S. Yao, TMS (The Minerals Metals & Materials Society), 2009, p. 429.
[10] B.-H. Lee, S.H. Park, S.-G. Hong, K.-T. Park, C.S. Lee, Mater. Sci. Eng. A 528 (2011) 1162–1172.
[11] S.R. Agnew, O. Duygulu, Int. J. Plasticity 21 (2005) 1161–1193.
[12] L. Jiang, J. Jonas, R. Mishra, A. Luo, A. Sachdev, S. Godet, Acta Mater. 55 (2007) 3899–3910.
[13] A. Jain, O. Duygulu, D.W. Brown, C.N. Tome, S.R. Agnew, Mater. Sci. Eng. A 486 (2008) 545–555.
[14] F.K. Abu-Farha, M.K. Khraisheh, J. Mater. Eng. Perform. 16 (2007) 192–199.
[15] J.A. Del Valle, M.T. Perez-Prado, O.A. Ruano, Metall. Mater. Trans. A 36 (2005) 1427–1438.
[16] H. Watanabe, H. Tsutsui, T. Mukai, M. Kohzu, S. Tanabe, K. Higashi, Int. J. Plasticity 17 (2001) 387–397.
[17] Y. Liu, X. Wu, Metall. Mater. Trans. A 37 (2006) 7–17.
[18] L.L. Chang, E.F. Shang, Y.N. Wang, X. Zhao, M. Qi, Mater. Charact. 60 (2009) 487–491.
[19] M. Wang, R. Xin, B. Wang, Q. Liu, Mater. Sci. Eng. A 528 (2011) 2941–2951.
[20] L. Jin, D.L. Lin, D.L. Mao, X.Q. Zeng, B. Chen, W.J. Ding, Mater. Sci. Eng. A 423 (2006) 247.
[21] Q. Miao, L. Hu, X. Wang, E. Wang, J. Alloys Compd. 493 (2010) 87–90.
[22] L. Jin, J. Dong, R. Wang, L.M. Peng, Mater. Sci. Eng. A 527 (2010) 1970–1974.
[23] A.S. Khan, A. Pandey, T. Gnaupel-Herold, R.K. Mishra, Int. J. Plasticity 27 (2011) 688–706.
[24] X. Huang, K. Suzuki, A. Watazu, I. Shigematsu, N. Saito, J. Alloys Compd. 479 (2009) 726–731.
[25] M.R. Barnett, A.G. Beer, D. Atwell, A. Oudin, Scripta Mater. 51 (2004) 19–24.
[26] R. Cottam, J. Robson, G. Lorimer, B. Davis, Mater. Sci. Eng. A 485 (2008) 375–382.
[27] C.D. Yim, Y.M. Seo, B.S. You, Met. Mater. Int. 15 (2009) 683.
[28] J.W. Christian, S. Mahajan, Prog. Mater. Sci. 39 (1995) 1–157.
[29] H.T. Jeong, T.K. Ha, J. Mater. Process. Technol. 187–188 (2007) 559–561.
[30] M.T. Pérez-Prado, O.A. Ruano, Scripta Mater. 46 (2002) 149–155.
[31] T. Perez-Prado, O.A. Ruano, Scripta Mater. 48 (2003) 59–64.
[32] J.J. Nah, H.G. Kang, M.Y. Huh, O. Engler, Scripta Mater. 58 (2008) 500–503.
[33] K.H. Kim, D.N. Lee, Acta Mater. 49 (2001) 2583–2595.
[34] H.G. Kang, M.Y. Huh, S.H. Park, O. Engler, Steel Res. Int. 79 (2008) 489–496.
[35] H.G. Kang, J.K. Kim, M.Y. Huh, O. Engler, Mater. Sci. Eng. A 452–453 (2007) 347–358.